INVESTIGATION ON TRANSIENT RESPONSES OF A PIEZOELECTRIC CRACK BY USING DURBIN AND ZHAO METHODS FOR NUMERICAL INVERSION OF LAPLACE TRANSFORMS

Y.-S. Ing * **H.-F. Liao**

Department of Aerospace Engineering
Tamkang University
Taipei, Taiwan 25137, R.O.C.

ABSTRACT

This study applies the numerical inversion of Laplace transform methods to study the piezoelectric dynamic fracture problem, recalculating Chen and Karihaloo's [1] analysis on the transient response of a impermeable crack subjected to anti-plane mechanical and in-plane electric impacts. Three numerical methods were adopted for calculating the dynamic stress intensity factor: Durbin method, Zhao method 1, and Zhao method 2. The results obtained were more accurate than the results in Chen and Karihaloo's [1] study. Through the calculation, this study presents a better range of parameters for the above three methods, and compares the advantages and disadvantages of each method in detail.

Keywords: Piezoelectric, Crack, Transient, Inversion, Laplace transform.

1. INTRODUCTION

Recently, with the development of materials and advances in manufacturing technology, piezoelectric materials are becoming increasingly common. However, most piezoelectric materials currently known are constructed from brittle substances, and are prone to brittle fracture when applied in areas of vibration. Therefore, research concerning piezoelectric structural damage is extremely vital. Numerous researchers have used Laplace transform and the inversion of Laplace transform as the primary tools for analyzing the dynamic fractures in piezoelectric materials. However, using the analytical inversion of Laplace transform during analysis makes the mathematical composition exceedingly complicated and difficult, and therefore only applicable to relatively simple geometric structures. Using the numerical inversion of Laplace transform for calculation in complex problems is more practical.

Over twenty different numerical methods for dealing with the inverse Laplace transform are proposed in the literature, and their application principles differ. For example, Gaussian quadrature has been used as the foundation for the numerical inversion of Laplace transform [2]; as have the methods from orthogonal functions [3-5]. Numerous studies are related to the numerical inversion of the Laplace transform obtained using the Fourier series [6-10]. There have also been numerous crucial studies and reviews related to the numerical inversion of Laplace transform [11-21].

Though numerous methods exist for the numerical inversion of Laplace transform, Narayanan and Beskos [22] already applied eight numerical inversions of Laplace transform to linear dynamic problems, and systematically discussed and calculated their efficiency. Their results demonstrated that Durbin [7] was the best method. The Durbin method [7] can obtain dependable results for both long and short time for most cases, but requires a relatively longer period of time for calculation. Zhao [20] proposed a new method for the numerical inversion of Laplace transform. He contended that the Durbin method [7] was unable to accurately calculate long-term transient responses when applied to dynamic issues in elastic-piezoelectric laminates, and that this new method resolved the disadvantages of Durbin [7] by being able to also provide reliable results for long-term responses. Because the ability to precisely calculate the numerical inversion of Laplace transform is a crucial part of studying the transient response of piezoelectric materials, this study used both Durbin [7] and Zhao methods [20] to the transient response of a piezoelectric crack, reanalyzing and recalculating the problem examined by Chen and Karihaloo [1]. This study also provided a detailed comparison of the properties, strengths, and weaknesses of each of the three methods, ultimately comparing the results of this study with analysis in prior studies to verify the accuracy of this study's calculations. Furthermore, this study also suggested preferable parameters for applying Durbin [7] and Zhao [20] methods to calculate the transient response of wave propagation in piezoelectric materials.

* Corresponding author (ysing@mail.tku.edu.tw)

DOI : 10.1017/jmech.2013.45

2. THE NUMERICAL INVERSION OF LAPLACE TRANSFORMS

2.1 Durbin Method

Let $f(t)$ be a function of time t, with $f(t) = 0$ for $t < 0$. The Laplace transform pair is defined by

$$\overline{f}(s) = \int_0^{\infty} e^{-st} f(t)\, dt \,, \tag{1}$$

$$f(t) = \frac{1}{2\pi i} \int_{c-i\infty}^{c+i\infty} e^{st} \overline{f}(s)\, ds \,, \tag{2}$$

where s is the complex transform parameter, c is a positive constant, and i is the imaginary unit. Durbin [7] derived the approximation formula

$$f(t) = \frac{2e^{\alpha t}}{T} \left\{ -\frac{1}{2} \mathrm{Re}\left[\overline{f}(\alpha) \right] + \sum_{k=0}^{\infty} \left(\mathrm{Re}\left[\overline{f}\left(\alpha + i\frac{2k\pi}{T} \right) \right] \cos\left(\frac{2\pi k t}{T} \right) - \mathrm{Im}\left[\overline{f}\left(\alpha + i\frac{2k\pi}{T} \right) \right] \sin\left(\frac{2\pi k t}{T} \right) \right) \right\} \,, \tag{3}$$

for $0 \le t \le T$. Generally, T is taken as the time length of inversion, and $\alpha T = 5$ to 10.

2.2 Zhao Method 1

Zhao [20] developed a new approach for the numerical inversion of Laplace transforms. Two formulas were derived based on the approximations of linear functions and Subbotin-splines. The author also believed that the new method can achieve a more reliable inversion than Durbin method for long time inversions. The proposed linear approximation to $f(t)$, named "Zhao method 1", can be written as

$$f(0) = \sum_{k=1}^{\infty} \frac{F_{k+1} + F_k}{2\pi} \Delta_k \,, \tag{4}$$

$$f(t) = \frac{e^{\alpha t}}{\pi t^2} \sum_{k=1}^{\infty} \left[\frac{F_{k+1} - F_k}{\Delta_k} (\cos \omega_{k+1} t - \cos \omega_k t) - \frac{G_{k+1} - G_k}{\Delta_k} (\sin \omega_{k+1} t - \sin \omega_k t) \right], \quad \text{for } t > 0 \,, \tag{5}$$

where $F_k = \mathrm{Re}\left[\overline{f}(\alpha + i\omega_k) \right]$, $G_k = \mathrm{Im}\left[\overline{f}(\alpha + i\omega_k) \right]$, $\Delta_k = \omega_{k+1} - \omega_k$, and $\omega_1 = 0$.

2.3 Zhao Method 2

If the functions $\mathrm{Re}\left[\overline{f}(\alpha + i\omega) \right]$ and $\mathrm{Im}\left[\overline{f}(\alpha + i\omega) \right]$ are approximated with Subbotin quadratic splines [23], the approximation to $f(t)$, named "Zhao method 2", can be expressed as

$$f(0) = \frac{1}{\pi} \sum_{k=1}^{n} \left[F_k + \frac{\Delta k}{24} (Z_{k+1} - Z_k) \right] \Delta k \,, \tag{6}$$

$$f(t) = \frac{e^{\alpha t}}{\pi} \left\{ \frac{1}{t} p_1(t) + \frac{1}{t^2} p_2(t) - \sum_{k=1}^{n} \frac{1}{t^3 \Delta k} \left[(Z_{k+1} - Z_k)(\sin\omega_{k+1} t - \sin\omega_k t) + (Y_{k+1} - Y_k)(\cos\omega_{k+1} t - \cos\omega_k t) \right] \right\}, \quad \text{for } t > 0 \,, \tag{7}$$

where

$$p_1(t) = \left[F_n + \frac{1}{8}(Z_n + 3Z_{n+1}) \Delta_n \right] \sin\omega_{n+1} t + \frac{1}{8}(Y_2 + 3Y_1)\, \Delta_1 - G_1 + \left[G_n + \frac{1}{8}(Y_n + 3Y_{n+1})\, \Delta_n \right] \cos\omega_{n+1} t \,,$$

$$p_2(t) = -Z_1 + Z_{n+1} \cos\omega_{n+1} t - Y_{n+1} \sin\omega_{n+1} t \,,$$

$$F_k = \mathrm{Re}\left[\overline{f}(\alpha + i\tau_k) \right], \quad G_k = \mathrm{Im}\left[\overline{f}(\alpha + i\tau_k) \right],$$

$$\tau_k = \frac{1}{2}(\omega_{k+1} + \omega_k) \,,$$

$$3\Delta_1 Z_1 + \Delta_1 Z_2 = 8(F_1 - F_0) \,,$$

$$\Delta_{k-1} Z_{k-1} + 3(\Delta_k + \Delta_{k-1}) Z_k + \Delta_k Z_{k+1} = 8(F_k - F_{k-1}) \,, \quad (k = 2, 3, ..., n) \,,$$

$$3\Delta_n Z_{n+1} + \Delta_n Z_n = 8(F_{n+1} - F_n) \,,$$

$$F_0 = \mathrm{Re}\left[\overline{f}(\alpha + i\omega_1) \right],$$

$$F_{n+1} = \mathrm{Re}\left[\overline{f}(\alpha + i\omega_{n+1}) \right],$$

$$3\Delta_1 Y_1 + \Delta_1 Y_2 = 8(G_1 - G_0) \,,$$

$$\Delta_{k-1} Y_{k-1} + 3(\Delta_k + \Delta_{k-1}) Y_k + \Delta_k Y_{k+1} = 8(G_k - G_{k-1}) \,, \quad (k = 2, 3, ..., n) \,,$$

$$3\Delta_n Y_{n+1} + \Delta_n Y_n = 8(G_{n+1} - G_n) \,,$$

$$G_0 = \mathrm{Im}\left[\overline{f}(\alpha + i\omega_1) \right],$$

$$G_{n+1} = \mathrm{Im}\left[\overline{f}(\alpha + i\omega_{n+1}) \right].$$

3. DYNAMIC INTENSITIES OF AN IMPERMEABLE PIEZOELECTRIC CRACK

3.1 Statement of the Problem

The specific geometry to be considered here is an infinite piezoelectric medium containing a finite crack of length of $2a$, as shown in Fig. 1. For $t < 0$, the medium is stress free and at rest. At time $t = 0$, arbitrary mechanical and electrical impacts act at the impermeable crack faces. Assume that the z-axis is the poling

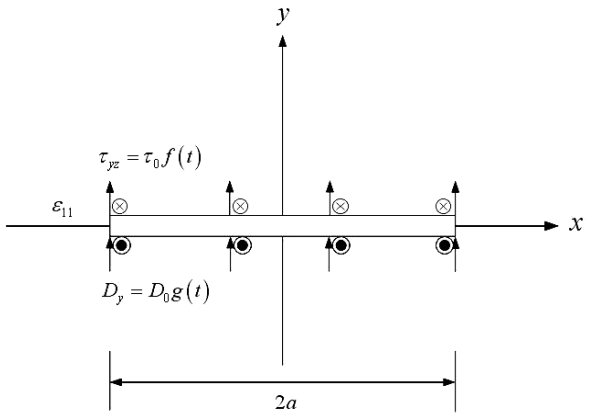

Fig. 1 Configuration and coordinate systems of a piezoelectric crack subjected to mechanical and electric impacts

direction, and only the out-of-plane displacement and the in-plane electric fields are considered. The dynamic anti-plane governing equations for a hexagonal piezoelectric material can be described by

$$c_{44}\nabla^2 w + e_{15}\nabla^2\phi = \rho\ddot{w} , \tag{8}$$

$$e_{15}\nabla^2 w - \varepsilon_{11}\nabla^2\phi = 0 , \tag{9}$$

where $w = w(x, y)$ is the anti-plane displacement in the z-direction (which is assumed to aligned with the hexagonal symmetry axis), $\phi = \phi(x, y)$ is the electric potential, c_{44} is the elastic modulus measured in a constant electric field, ε_{11} is the dielectric permittivity measured at a constant strain, e_{15} is the piezoelectric constant, and ρ is the material density. $\nabla^2 = \partial^2/\partial x^2 + \partial^2/\partial y^2$ is the in-plane Laplacian, and a dot denotes material time derivative.

The constitutive equations for the piezoelectric material can be expressed as

$$\tau_{xz} = c_{44}\,\partial w/\partial x + e_{15}\,\partial\phi/\partial x , \tag{10}$$

$$\tau_{yz} = c_{44}\,\partial w/\partial y + e_{15}\,\partial\phi/\partial y , \tag{11}$$

$$D_x = e_{15}\,\partial w/\partial x - \varepsilon_{11}\,\partial\phi/\partial x , \tag{12}$$

$$D_y = e_{15}\,\partial w/\partial y - \varepsilon_{11}\,\partial\phi/\partial y . \tag{13}$$

The boundary conditions of the present problem can be written as

$$\tau_{yz}(x,\ 0,\ t) = \tau_0 f(t) ,\quad |x| < a , \tag{14}$$

$$D_y(x,\ 0,\ t) = D_0 g(t) ,\quad |x| < a , \tag{15}$$

$$w(x, 0, t) = \phi(x, 0, t) = 0 ,\quad |x| > a , \tag{16}$$

$$\lim_{y\to\pm\infty} \tau_{yz}(x, y, t) = \lim_{y\to\pm\infty} D_y(x, y, t) = 0 . \tag{17}$$

3.2 Dynamic Intensities in the Laplace Transform Domain

Using the method proposed by Loeber and Sih [24], the above problem can be solved in the Laplace transform domain. In this paper, the authors obtained the same analytical solution as that of Chen and Karihaloo [1]. Finally, the dynamic stress intensity factor and the dynamic electric displacement intensity factor in the Laplace transform domain can be expressed as

$$\bar{k}_3^{\tau}(s) = \sqrt{\pi a}\left[\tau_0\Phi(1,\ s)\,\bar{f}(s) + \frac{D_0 e_{15}}{\varepsilon_{11}}\Phi(1,\ s)\bar{g}(s) - \frac{D_0 e_{15}}{\varepsilon_{11}}\,\bar{g}(s)\right] , \tag{18}$$

$$\bar{k}_3^{D}(s) = \sqrt{\pi a} D_0 \bar{g}(s) . \tag{19}$$

The functions $\bar{f}(s)$ and $\bar{g}(s)$ are Laplace transforms of excitations $f(t)$ and $g(t)$, respectively. Moreover, the function $\Phi(1, s)$ is determined by the following Fredholm integral equation of the second kind

$$\Phi(\xi, s) + \int_0^1 K(\xi, \eta, s)\Phi(\eta, s)\, d\eta = \sqrt{\xi} . \tag{20}$$

The kernel of the integral equation is

$$K(\xi, \eta, s) = \sqrt{\xi\eta}\int_0^{\infty}\left[a\gamma(\tau/a, s) - \tau\right] J_0(\tau\xi) J_0(\tau\eta)\, d\tau , \tag{21}$$

in which $\gamma(\tau, s) = (\tau^2 + s^2/c_s^2)^{1/2}$, $c_s = \sqrt{\mu/\rho}$, $\mu = c_{44} + e_{15}^2/\varepsilon_{11}$, and $J_0(\ )$ is the zero-order Bessel function of the first kind.

3.3 Acceleration of Convergence for Kernel Function

The direct calculation of the kernel function as expressed in Eq. (21) is difficult to converge. The suggestion given by Loeber and Sih [24] can be used to accelerate the convergence of this integral. Rewriting the kernel function $K(\xi, \eta, s)$ in the following form:

$$K(\xi,\ \eta,\ s) = \sqrt{\xi\eta}\left\{\frac{a^2 s^2}{2c_s^2}\int_0^{\infty}\frac{\tau}{\tau^2 + (ma)^2} J_0(\tau\xi)\ J_0(\tau\eta)\, d\tau - \int_0^{\infty}\tau\gamma^*\left(\frac{\tau}{a}, s\right) J_0(\tau\xi)\ J_0(\tau\eta)\, d\tau\right\} , \tag{22}$$

where m is set to 0.5 ~ 1 and

$$\gamma^*(\tau, s) = \frac{s^2}{2c_s^2(\tau^2 + m^2)} - \sqrt{1 + \frac{s^2}{c_s^2\tau^2}} + 1 . \tag{23}$$

The first integral in Eq. (22) is explicit integrable, and that the convergence of the second integral accelerates from $O(\tau^{-2})$ to $O(\tau^{-4})$. The final form of the kernel is

$$K(\xi, \eta, s) = \begin{cases} \sqrt{\xi\eta}\left[\frac{a^2 s^2}{2c_s^2} I_0(ma\eta) K_0(ma\xi) - \int_0^\infty \tau\gamma^*\left(\frac{\tau}{a}, s\right) J_0(\tau\xi) J_0(\tau\eta) d\tau\right], & (0 < \eta < \xi), \\ \sqrt{\xi\eta}\left[\frac{a^2 s^2}{2c_s^2} I_0(ma\xi) K_0(ma\eta) - \int_0^\infty \tau\gamma^*\left(\frac{\tau}{a}, s\right) J_0(\tau\xi) J_0(\tau\eta) d\tau\right], & (0 < \xi < \eta), \end{cases} \tag{24}$$

where $I_0(\ )$ and $K_0(\ )$ are the zero-order modified Bessel functions of the first and the second kinds, respectively.

4. NUMERICAL RESULTS AND DISCUSSION

4.1 Numerical Solutions to the Fredholm Integral Equation

This study used Gaussian quadrature to resolve the Fredholm integral equation in Eq. (20). From Gaussian quadrature, Eq. (20) can be expressed as

$$\Phi(\xi, s) + \frac{1}{2}\sum_{i=1}^{n} w_i K(\xi, \eta_i, s)\Phi(\eta_i, s) = \sqrt{\xi} . \tag{25}$$

where w_i are the weighting factors, η_i are the integration points, and n is the number of Gaussian quadrature points. Here, the 24-point Gaussian quadrature was adopted. After each of the Gaussian quadrature points η_1 to η_{24} replaced ξ in Eq. (25), 24 simultaneous equations could be obtained

$$\sum_{i=1}^{24}\left[\frac{1}{2} w_i K(\eta_j, \eta_i, s) + \delta_{ij}\right]\Phi(\eta_i, s) = \sqrt{\eta_j} , \quad j = 1, 2, 3, \ldots 24 , \tag{26}$$

where

$$\delta_{ij} = \begin{cases} 1, & \text{if } i = j , \\ 0, & \text{if } i \neq j . \end{cases}$$

After the simultaneous equations in Eq. (26) resolved $\Phi(\eta_i, s)$, $\Phi(1, s)$ in Eq. (18) can use Eq. (25) to calculate

$$\Phi(1, s) = 1 - \frac{1}{2}\sum_{i=1}^{24} w_i K(1, \eta_i, s)\Phi(\eta_i, s) . \tag{27}$$

Once $\Phi(1, s)$ is determined, the dynamic stress intensity factor $k_3^{\tau}(t)$ can be obtained by inverting the Laplace transform of Eq. (18).

4.2 Numerical Results

During numerical calculation, the load function is assumed to be $f(t) = g(t) = H(t)$, where $H(t)$ is the Heaviside function. To verify the accuracy of the numerical inversion of Laplace transform, a special case from the literature was first calculated: The piezoelectric constant $e_{15} = 0$. The results of this study could be compared to the analysis by Ing and Ma [25] regarding purely elastic materials. The parameters during calculation were set to $T = 75$ and $\alpha T = 5$, and the Δ_k in Zhao methods was assumed to be a constant step. Durbin method added 300 terms, while Zhao methods 1 and 2 added 600. The results are displayed in Fig. 2. The results for Zhao methods 1 and 2 in Fig. 2 overlap, and the transient values of the stress intensity factor for all three methods are extremely close to the analytical solution in Ing and Ma's study [25]. The maximum value of the non-dimensional stress intensity factor for purely elastic materials is $4/\pi$. Figure 2 shows that the maximum dynamic overshoot occurs at $c_s t / a = 2$ for the three methods, and that as the calculation time lengthens, the dynamic stress intensity factor quickly becomes a static value. These results differ significantly from the Fig. 2 results in Chen and Karihaloo's study [1] ($e_{15} D_0 / (\tau_0 \varepsilon_{11}) = 0$). This case demonstrates the exceptional accuracy of the results in this study.

Displaying the calculation results for the Durbin method using various total number of summations, Fig. 3 shows that when excluding the relatively inaccurate $N = 50$, the lines for $N = 300$, 500, and 1000 almost coincide. Therefore, when applying Durbin method to the piezoelectric material fracture problem in this study, $N = 300$ was sufficient to obtain accurate results. Figures 4 and 5 display the results for Zhao methods 1 and 2, respectively, using N different total numbers added. The figures demonstrate the similarity of the results of the two methods; errors were prevalent for $N = 300$ and $N = 500$, whereas $N = 600$, 1000, and 1500 completely coincided. Therefore, when applying Zhao methods 1 and 2 to this dynamic fracture problem, N must equal at least 600 to obtain more accurate solutions. This requires significantly more terms for calculation than Durbin method.

In the literature, the suggested value of the period T in Durbin method should be equal to the longest calculation time [7]. However, this study found that to create accurate numerical results with fewer terms, the set value of the period T should be even greater than the longest calculation time, and αT needs only to be set between 5 and 10 to obtain satisfactory results. To explain these results, Fig. 6 compared Durbin method calculated using different periods T, when $\alpha T = 5$ and $N = 300$. Figure 6 shows that latter period errors are significant when $T = 10$, but that the results for $T = 20$ and $T = 75$ were approximately similar. Therefore, better numerical solutions can be obtained when T is set at a greater value. Zhao [20] contended that Durbin method was insufficiently accurate when a long calculation time was used, primarily because the period was set too small. However, Fig. 6 demonstrates that when Durbin method is applied to this dynamic fracture problem with piezoelectric materials, lengthening the period T increases accuracy and calculation speed.

Figures 7 and 8 compared Zhao methods 1 and 2, respectively, using different T. The two figures show that when $T = 10$, the latter part of the results are more

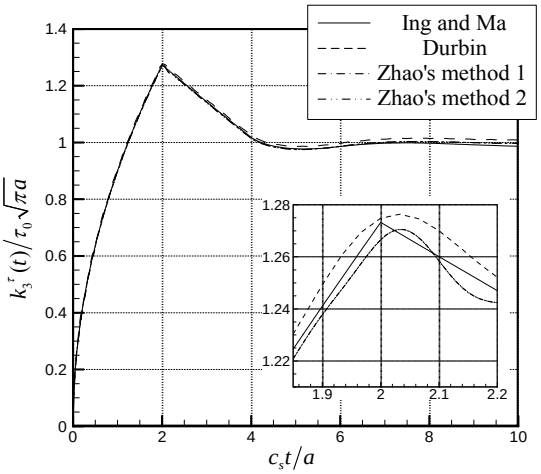

Fig. 2 Normalized dynamic stress intensity factors versus normalized time for purely elastic materials by different methods of Laplace transform inversion. ($T = 75$, $\alpha T = 5$)

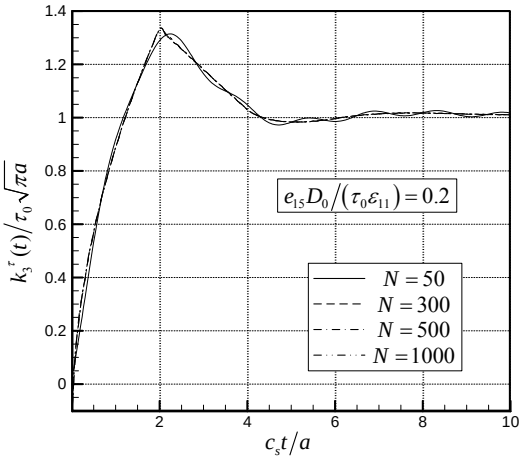

Fig. 3 Normalized dynamic stress intensity factors versus normalized time with various number of summations by Durbin method. ($T = 75$, $\alpha T = 5$)

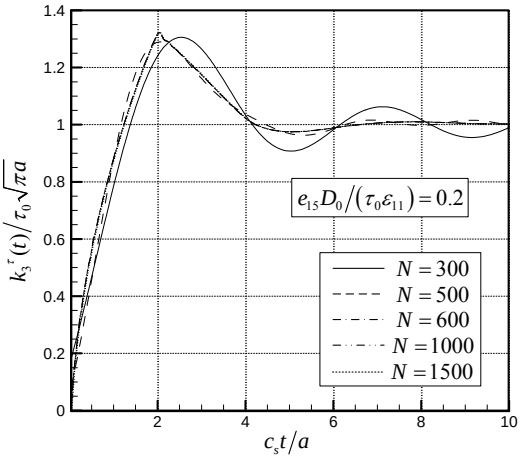

Fig. 4 Normalized dynamic stress intensity factors versus normalized time with various number of summations by Zhao method 1. ($T = 75$, $\alpha T = 5$, Δ_k = constant)

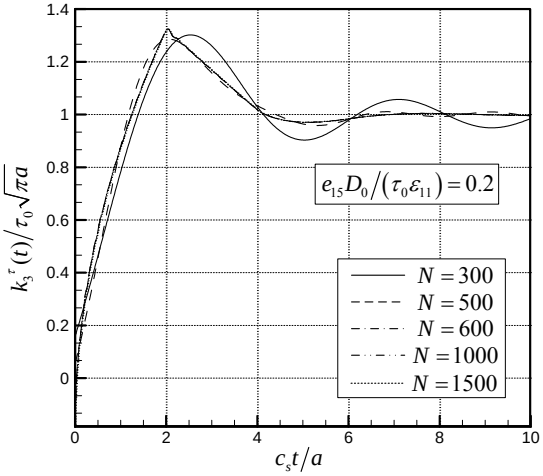

Fig. 5 Normalized dynamic stress intensity factors versus normalized time with various number of summations by Zhao method 2. ($T = 75$, $\alpha T = 5$, Δ_k = constant)

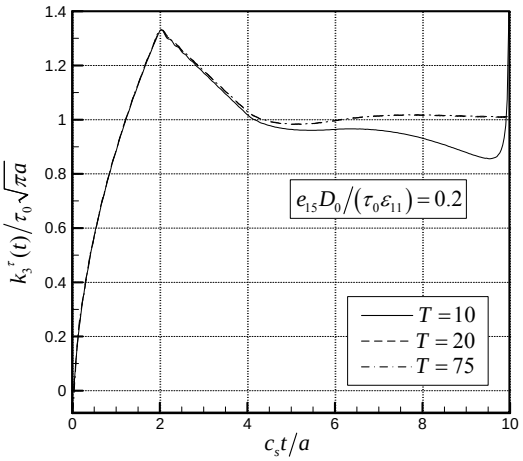

Fig. 6 Normalized dynamic stress intensity factors versus normalized time with various periods T by Durbin method. ($\alpha T = 5$, $N = 300$)

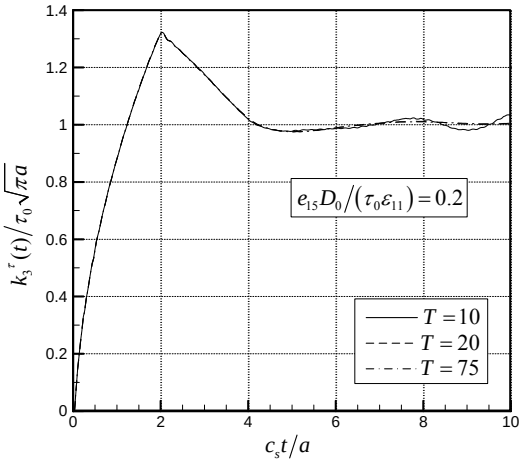

Fig. 7 Normalized dynamic stress intensity factors versus normalized time with various periods T by Zhao method 1. ($\alpha T = 5$, $N = 600$)

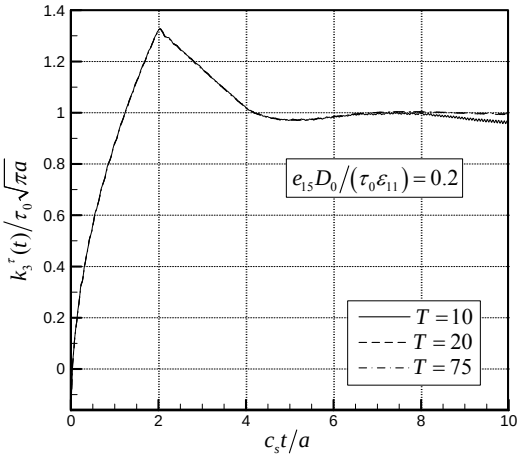

Fig. 8 Normalized dynamic stress intensity factors versus normalized time with various periods T by Zhao method 2. ($\alpha T = 5$, $N = 600$)

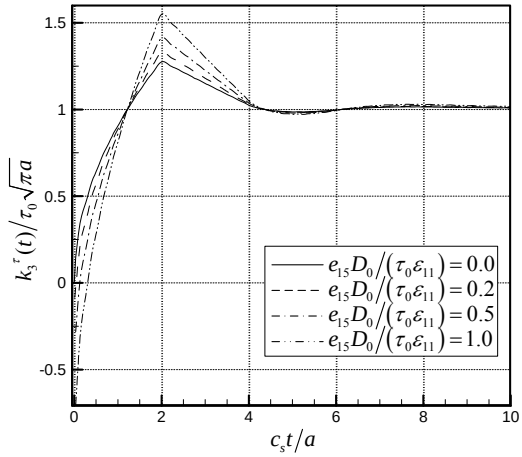

Fig. 9 Normalized dynamic stress intensity factors versus normalized time for various electro-mechanical loads by Durbin method. (T = 20, $\alpha T = 5$, $N = 300$)

volatile; indicating that when the calculation time is long, the inverse transform results will become inaccurate. The results for T = 20 and T = 75 are nearly identical. Therefore, when applying Zhao methods to the piezoelectric fracture problem in this study, a greater value T provides more accurate results. To understand the effect of T on the calculation results over a long time period, this study also calculated many different cases and discovered that for identical assumptions about period T, Zhao method 1 can calculate for the greatest amount of time while still obtaining better transient numerical results; followed by Durbin method, and finally by Zhao method 2. If numerical solutions with long calculation times are required, this study recommends setting T to greater than two times the longest calculation time when using Durbin method, and to approximately three times the longest calculation time when using Zhao method 2. Zhao method 1, however, only needs to be slightly greater than the longest calculation time. Although increasing T could affect the accuracy of short-time numerical results, the results in this study indicate that the effect is insignificant. Therefore, increasing the period is a feasible method for obtaining an accurate, long-time, transient numerical solution. If the accuracy required for short time results is also fairly rigorous, calculating the transient solutions separately according to time and setting different periods T for different calculations should be considered to obtain relatively accurate results.

Next, this study discusses the results of piezoelectric cracks subjected to electric displacement loads by explaining only the results calculated using Durbin method. Figure 9 displays the numerical results for the transient stress intensity factors of a piezoelectric crack subjected to electric displacement impact. The figure indicates that when load action is initiated, the stress intensity factor is induced immediately; and that the greater the electric displacement load, the greater the magnitude of the initial value. Furthermore, Fig. 9 demonstrates that when $c_s t / a \approx 0 \sim 1.2$, the electric displacement load will cause the stress intensity factor to decrease in value, indicating a electric field could retard the propagation of a crack. When $c_s t / a = 2$, the diffracted wave from the other tip of the crack had arrived at the crack tip, and the stress intensity factor is at its maximum value. Figure 9 also shows that variation in electric field magnitude has absolutely no effect on the time at which maximum stress intensity factor values occur. Because the time-dependent functions for stress and electric displacement loads are identical ($f(t) = g(t) = H(t)$), Eq. (18) can theoretically be rewritten as

$$\frac{k_3^{\tau}(t)}{\tau_0\sqrt{\pi a}} = \left[M(t)\left(1+\frac{D_0\, e_{15}}{\tau_0\, \varepsilon_{11}}\right) - \frac{D_0\, e_{15}}{\tau_0\, \varepsilon_{11}} \right], \qquad (28)$$

where $M(t)$ is the inverse Laplace transform for function $\Phi(1, s)\,\overline{f}(s)$. Because the maximum value occurs at $d\,M(t)/dt = 0$, and Eq. (28) shows that the ratio of $e_{15} D_0 / (\tau_0 \varepsilon_{11})$ is unrelated to this time. It means that the time at which the dynamic stress intensity factor reaches a maximum is absolutely unaffected by changes of the magnitude of electric displacement loads. Figure 9 further shows that when $c_s t / a \approx 1.2 \sim 4.2$, the increase in electric displacement load will actually increase the stress intensity factor value; indicating that at this point, a electric field will promote crack propagation. Subsequently, when $c_s t / a \approx 4.2 \sim 6.2$, the greater the electric displacement load, the smaller the stress intensity factor; thereby revealing an inverse trend. Therefore, the effect of the electric displacement load on dynamic stress intensity factors varies over time; electric displacement load may at times promote, and at other times retard, the propagation of a crack in piezoelectric materials.

For dynamic electric displacement intensity factors, Eq. (19) indicates that when $g(t) = H(t)$, $k_3^D(t) = D_0\sqrt{\pi a}H(t)$, meaning that dynamic electric displacement intensity factors immediately jump to a static solution the moment after load is applied. This phe-

nomenon is due to the assumption that the speed of electromagnetic waves is infinite; therefore, the moment that electric displacement load is applied, the electromagnetic wave effect is induced at the crack tip.

The above calculations all assumed the time-dependent load function $f(t) = g(t) = H(t)$. This study considers two special load forms in the following discussion. The first type supposes that $f(t) = g(t) = H(t) - H(c_s t / a - 6)$, or that the load is first applied at $t = 0$ and then removed at $c_s t / a = 6$. The numerical results from each of the three inverse Laplace transforms are displayed in Fig. 10. The figure shows that the results for Zhao methods 1 and 2 are relatively inaccurate, with especially volatile oscillations around $c_s t / a = 6$. Therefore, applying either of Zhao methods to this type of step load function creates inaccurate results. Figure 10 also shows that because the load was not reapplied at $c_s t / a \geq 6$, the stress intensity factor approaches zero as t approaches infinity. The second type of load assumes that $f(t) = g(t) = t/t_l\, H(t) - (t/t_l - 1)\, H(t - t_l)$, where t_l is the ramp time required for the load to increase from zero to τ_0 or D_0. Figure 11 displays the dynamic stress intensity factor results when Durbin method was applied to different ramp times. The figure indicates that the greater the ramp time, the slower the initial rate of increase for stress intensity factors, thus the lower the maximum peak value; and later, the maximum value was obtained.

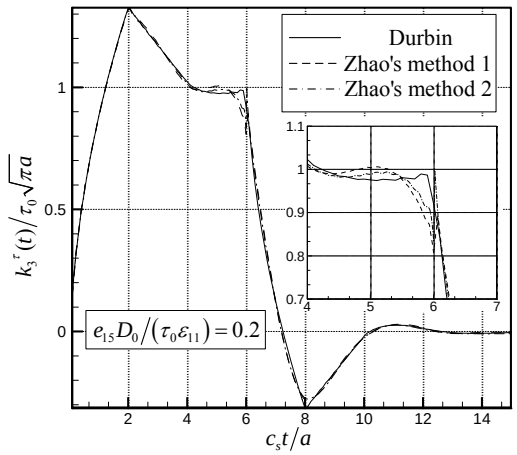

Fig. 10 Normalized dynamic stress intensity factors versus normalized time under step-loading condition by different methods of Laplace transform inversion. ($T = 30$, $\alpha T = 5$, $N = 300$ for Durbin method and $N = 600$ for Zhao methods)

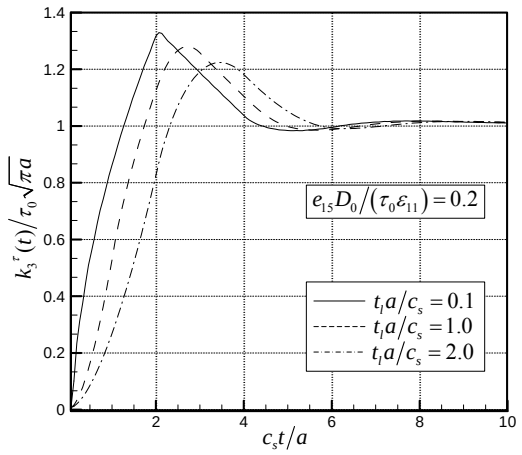

Fig. 11 Normalized dynamic stress intensity factors versus normalized time with various ramp time t_l by Durbin method. ($T = 20$, $\alpha T = 5$, $N = 300$)

5. CONCLUSIONS

In numerous studies, Laplace transforms have been used to solve the dynamic fracture problem with piezoelectric materials, for which accurately calculating the numerical inversion of Laplace transforms is crucial. This study successfully applied three numerical inversions of Laplace transform methods—Durbin method, Zhao method 1, and Zhao method 2—to the transient problem of a piezoelectric crack subjected to anti-plane mechanical and in-plane electric impacts. The conclusions drawn from the results of this study are as follows:

1. The transient numerical results of the problem can be achieved using three methods for the numerical inversion of Laplace transforms. The calculation figures demonstrate the effect of each diffracted wave on the crack tip stress intensity factor, and are compared with analytical solutions obtained by research on purely elastic materials to verify the accuracy of these results.
2. Depending on the time period, electric displacement load can either increase or decrease the transient stress intensity factor value, thereby retarding or promoting the propagation of the crack. This study also finds that electric displacement intensity factor depends only on the electric displacement load, and is unrelated to the mechanical stress load.
3. In prior studies, Durbin method was primarily believed to be unable to accurately calculate results over a long time; however, this study finds that simply increasing the setting for period T can correct this inefficiency. Though this change can slightly vary the results for short periods, they are still relatively accurate, and the calculation efficiency is still comparatively high with that of Zhao method 1 and Zhao method 2. This study also proposes recommended values for the time period settings of the three methods.
4. The numerical results produce a greater oscillation when Zhao methods are applied to a step-load case. If the total number of summations N does not continually increase, these two methods remain less accurate than Durbin method does.

ACKNOWLEDGMENTS

The authors gratefully acknowledge the financial support of this research by the National Science Council (Republic of China) under Grant NSC 96-2221-E-032-044-.

REFERENCES

1. Chen, Z. T. and Karihaloo, B. L., "Dynamic Response of a Cracked Piezoelectric Ceramic Under Arbitrary Electro-Mechanical Impact," *International Journal of Solids and Structures*, **36**, pp. 5125–5133 (1999).
2. Schmittroth, L. A., "Numerical Inversion of Laplace Transforms," *Communications of the ACM*, **3**, pp. 171–173 (1960).
3. Bellman, R. E., Kalaba, R. E. and Lockett, J., *Numerical Inversion of Laplace Transform*, American Elsevier, New York (1966).
4. Miller, M. K. and Guy, W. T., "Numerical Inversion of the Laplace Transform by Use of Jacobi Polynomials," *SIAM Journal on Numerical Analysis*, **3**, pp. 624–635 (1966).
5. Week, W. T., "Numerical Inversion of Laplace Transforms Using Laguerre Functions," *Journal of the Association for Computing Machinery*, **13**, pp. 419–429 (1966).
6. Dubner, H. and Abate, J., "Numerical Inversion of Laplace Transforms by Relating Them to the Finite Fourier Cosine Transform," *Journal of the Association for Computing Machinery*, **15**, pp. 115–123 (1968).
7. Durbin, F., "Numerical Inversion of Laplace Transforms: An Efficient Improvement to Dubner and Abate's Method," *The Computer Journal*, **17**, pp. 371–376 (1974).
8. Crump, K. S., "Numerical Inversion of Laplace Transforms Using a Fourier Series Approximation," *Journal of the Association for Computing Machinery*, **23**, pp. 89–96 (1976).
9. Albrecht, P. and Honig, G., "Numerical Inversion of Laplace Transforms: [Numerische Inversion Der Laplace-Transformierten]," *Angewandte Informatik*, **8**, pp. 336–345 (1977).
10. Honig, G. and Hirdes, U., "A Method for the Numerical Inversion of Laplace Transforms," *Journal of Computational and Applied Mathematics*, **10**, pp. 113–132 (1984).
11. Zakian, V. and Coleman, R., "Numerical Inversion of Rational Laplace Transforms," *Electronics Letters*, **7**, pp. 777–778 (1971).
12. Singhal, K., Vlach, J. and Vlach, M., "Numerical Inversion of Multidimensional Laplace Transform," *Proceedings of the IEEE*, **63**, pp. 1627–1628 (1975).
13. Hosono, T., "Numerical Inversion of Laplace Transform and Some Applications to Wave Optics," *Radio Science*, **16**, pp. 1015–1019 (1981).
14. Therapos, C. P. and Diamessis, J. E., "Numerical Inversion of a Class of Laplace Transforms," *Electronics Letters*, **18**, pp. 620–622 (1982).
15. Shih, D. H., Shen, R. C. and Shiau, T. C., "Numerical Inversion of Multidimensional Laplace Transforms," *International Journal of Systems Science*, **18**, pp. 739–742 (1987).
16. Kwok, Y. K. and Barthez, D., "An Algorithm for the Numerical Inversion of Laplace Transforms," *Inverse Problems*, **5**, pp. 1089–1095 (1989).
17. Evans, G. A., "Numerical Inversion of Laplace Transforms Using Contour Methods," *International Journal of Computer Mathematics*, **49**, pp. 93–105 (1993).
18. Wu, J. L., Chen, C. H. and Chen, C. F., "Numerical Inversion of Laplace Transform Using Haar Wavelet Operational Matrices," *IEEE Transactions on Circuits and Systems I: Fundamental Theory and Applications*, **48**, pp. 120–122 (2001).
19. Abate, J. and Valkó, P. P., "Multi-Precision Laplace Transform Inversion," *International Journal for Numerical Methods in Engineering*, **60**, pp. 979–993 (2004).
20. Zhao, X., "An Efficient Approach for the Numerical Inversion of Laplace Transform and its Application in Dynamic Fracture Analysis of a Piezoelectric Laminate," *International Journal of Solids and Structures*, **41**, pp. 3653–3674 (2004).
21. Milovanović, G. V. and Cvetković, A. S., "Numerical Inversion of the Laplace Transform," *Electronics and Energetics*, **18**, pp. 515–530 (2005).
22. Narayanan, G. V. and Beskos, D. E., "Numerical Operational Methods for Time-Dependent Linear Problems," *International Journal for Numerical Methods in Engineering*, **18**, pp. 1829–1854 (1982).
23. Cheney, W. and Kincaid, D., *Numerical Mathematics and Computing*, 2nd Edition, Brooks/Cole Publishing Company, Monterey, (1985).
24. Loeber, J. F. and Sih, G. C., "Diffraction of Antiplane Shear Waves by a Finite Crack," *Journal of the Acoustical Society of America*, **44**, pp. 90–98 (1968).
25. Ing, Y. S. and Ma, C. C., "Dynamic Fracture Analysis of a Finite Crack Subjected to an Incident Horizontally Polarized Shear Wave," *International Journal Solids Structures*, **34**, pp. 895–910 (1997).

(Manuscript received October 30, 2012,
accepted for publication March 14, 2013.)